3-D LEAST SQUARES TRACKING IN TIME-RESOLVED TOMOGRAPHIC RECONSTRUCTION OF DENSE FLOW MARKER FIELDS

Patrick Westfeld and Hans-Gerd Maas

Institute of Photogrammetry and Remote Sensing
Technische Universität Dresden, Helmholtzstr. 10, D-01062 Dresden, Germany
patrick.westfeld@tu-dresden.de, www.tu-dresden.de/ipf/photo/

Commission V, WG V/1

KEY WORDS: PIV Processing, Tomographic Reconstruction, Tracking, Flow Measurement Techniques

ABSTRACT:

Flow measurement techniques determine velocity vector fields in liquid or gas flows. In fluid mechanics, many methods are based on seeding particles to visualize the flow imaged by an adequate camera system. The tomo-PIV (tomographic particle image velocimetry) technique presented in this paper generates time-resolved volumetric reconstructions of a particle constellation from a limited number of synchronized camera views. The advantage of tomo-PIV in contrast to the established 3-D PTV (particle tracking velocimetry) technique is its insensitivity to high seeding densities. While 3-D PTV comes with the necessity to detect, identify and match individual particles for establishing multi-image and multi-temporal correspondences, tomo-PIV facilitates volume-based tracking schemes applied to voxel cuboids filled with particles. The paper presents improved photogrammetric techniques for the determination of 3-D flow velocity fields. This includes a multi-camera system configuration and calibration, approaches for a full tomographic reconstruction in gas and liquid and 3-D least squares tracking for volume-based tracking in object space.

1. INTRODUCTION

Elsinga et al. (2005) have proposed an approach to 3-D PIV, which is based on a tomographic reconstruction of the observation volume and subsequent 3-D cross correlation in time-resolved voxel data. Tomographic PIV generates a tomographic reconstruction of a particle constellation from a limited number of camera views, for instance by applying Herman and Lent's (1976) MART algorithm (multiplicative algebraic reconstruction technique). 3-D velocity field information can be obtained from time-resolved voxel data by dividing the data into cuboids of a pre-defined size and tracking these cuboids. Herein, 3-D cross correlation is a straightforward enhancement when advancing from 2-D PIV to 3-D PIV. Disadvantages of both, MART and 3-D cross correlation can be seen in the computational effort causing rather long processing times.

Putze & Maas (2008) and Maas et al. (2009) have already introduced more efficient approaches on volumetric reconstruction and particle tracking. This article summarizes the efforts of our working group and presents results which prove the suitability of photogrammetric techniques in voxel data sequences analysis.

2. SENSOR AND DATA

The tomographic reconstruction methods and the cuboid tracking have been implemented and tested in two different experimental setups. First, a vortex ring in a water tank is illuminated by a 3-D laser beam device. A rotating mirror generates parallel light sheet planes with a thickness of 10 mm. This volume of about (10×10×1) cm^3 is recorded by a system of four synchronized high speed cameras (1024×1024 pixel, 1000 fps) equipped with telecentric lenses (Fig. 1 and 2). Neutrally buoyant seeding particles are injected into the center of a vortex generator. See (Kitzhofer et al., 2009) for detailed specifications of this experimental setup.

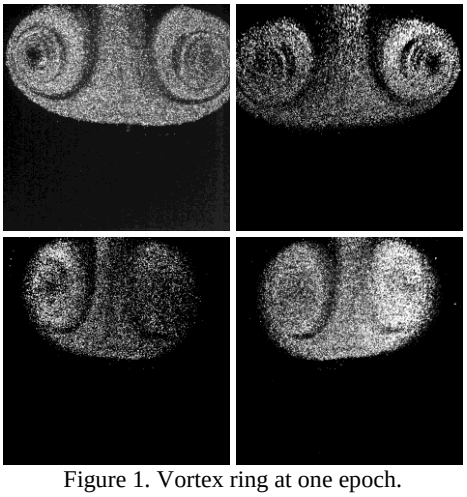

Figure 1. Vortex ring at one epoch.

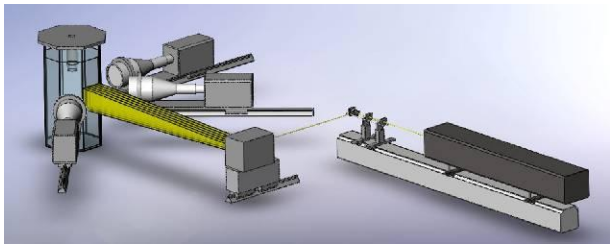

Figure 2. Experimental setup with telecentric lenses (Kitzhofer et al., 2009).

Using telecentric lenses results in a parallel projection for the observed volume. A consideration of multi-media geometries is

not necessary for this special case, but the collinearity equations have to be adapted to a parallel projection in space:

$$x' = pp_x + K(r_{11}(X - X_0) + r_{21}(Y - Y_0) + r_{31}(Z - Z_0)) + \Delta x' \quad (1)$$
$$y' = pp_y + K(r_{12}(X - X_0) + r_{22}(Y - Y_0) + r_{32}(Z - Z_0)) + \Delta y'$$

where	cc:	Focal length	X_0,Y_0,Z_0:	Projection center
	x',y':	Image point	X,Y,Z:	Object point
	pp_x,pp_y:	Principal point	$r_{r,c}$:	Elements of a rotation matrix **R**
	$\Delta x', \Delta y'$:	Correction functions		

The four-camera system was calibrated by taking image sequences of a target, which was moved through the observation volume by a 3-D translation stage. From these reference positions and their respective image coordinates, the orientation parameters of each camera were determined in a parallel projection telecentric optics camera model (Eq. 1). The transition of the optical paths from the camera through the plain glass interface into the water could be neglected due to the fact that the cameras were equipped with telecentric lenses warranting a parallel projection rather than central perspective projection.

In a second experimental configuration, different particle constellations in a water basin are illuminated by a fiber optic light source and are captured by a four-camera-recording-system (1000×1000 pixel; Fig. 3). Herein, the cameras are equipped with central perspective lenses and are able to capture images with an interval of a few microseconds between two images in a triggered double exposure mode.

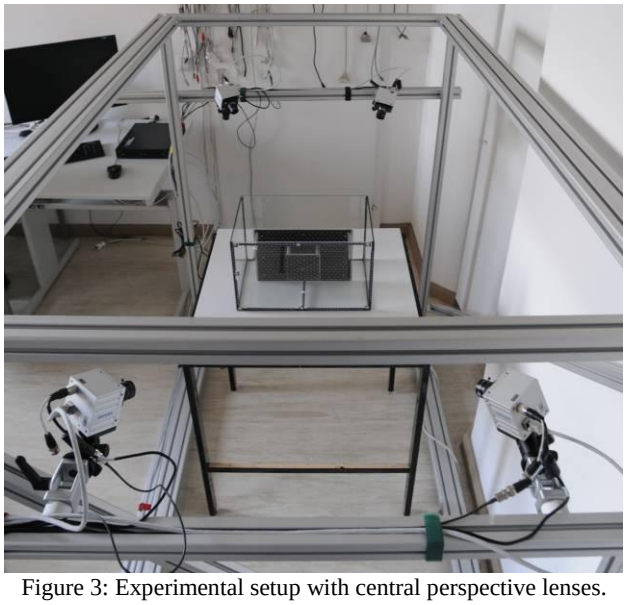

Figure 3: Experimental setup with central perspective lenses.

If used in one medium only, the well-known collinearity equations describe the image ray paths:

$$x' = pp_x + cc\frac{r_{11}(X - X_0) + r_{21}(Y - Y_0) + r_{31}(Z - Z_0)}{r_{13}(X - X_0) + r_{23}(Y - Y_0) + r_{33}(Z - Z_0)} + \Delta x' \quad (2)$$
$$y' = pp_y + cc\frac{r_{12}(X - X_0) + r_{22}(Y - Y_0) + r_{32}(Z - Z_0)}{r_{13}(X - X_0) + r_{23}(Y - Y_0) + r_{33}(Z - Z_0)} + \Delta y'$$

This collinearity of the image point, the projection center and the object point is not given if particles are observed in liquids by central perspective lenses. To consider the multimedia geometry, two kinds of ray tracing approaches are implemented; a forward (FRT) and a backward ray tracing (BRT).

For a spatial intersection, the complete image ray path has to be reconstructed (Fig. 4): (i) Intersect the image ray with the first interface Σ_1 and calculate the piercing point $\mathbf{P_1}$. (ii) Calculate the angle of incidence α_1 resp. the angle of refraction α_2 in accordance to Snell's law using the refraction indices of the media air and glass. (iii) Calculate the refracted direction vector using the incoming direction vector, the surface normal vector of $\mathbf{P_1}$ in Σ_1 and the relative refractive index. (iv) Repeat i-iii for the second refraction at the following interface Σ_2. (v) Finally, the coordinates of an object point **X** can be calculated by intersecting the reconstructed ray with a desired depth layer resp. with two (or more) other ray paths. For a spatial resection (BRT) the coordinates of the piercing points $\mathbf{P_1}$ resp. $\mathbf{P_2}$ have to be calculated sequentially in an iterative manner by solving a non-linear system of equations of conditions. These constraints are: (i) The piercing point $\mathbf{P_{1,2}}$ is located on the plane $\Sigma_{1,2}$. (ii) Snell's law has to be fulfilled. (iii) The normal vector of $\mathbf{P_{1,2}}$ in $\Sigma_{1,2}$ as well as the incident and reflected ray are coplanar. A detailed mathematic description for FRT and BRT including all necessary equations is given in (Mulsow, 2010).

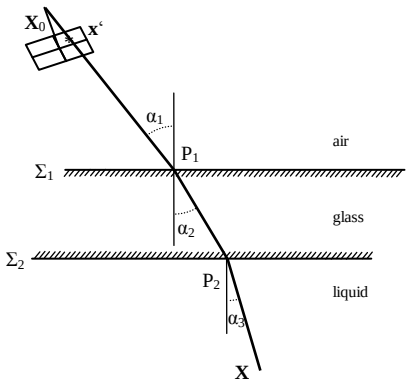

Figure 4. Multimedia geometry.

Mulsow's (2010) flexible multimedia bundle approach is used to determine the interior and exterior camera parameters as well as the media and interface parameters. The latter, namely the refractive indices and the normal vectors of the planes, are necessary to reconstruct the image ray paths through the different media gas, glass and liquid as described above.

3. VOLUMETRIC RECONSTRUCTION

3.1 Principle

Tomographic particle image velocimetry (Tomo-PIV, Elsinga et al., 2005) generates a tomographic reconstruction of a 3-D particle constellation from typically four camera views. and has the potential to solve the spatial resolution limit in 3-D PTV (particle tracking velocimetry), which is set by ambiguities occurring at high seeding densities. A reconstruction can be performed by a MART (multiplicative algebraic reconstruction technique; Herman & Lent, 1976):

1. Project every voxel into the first image space, using the model equations 1 resp. 2. The voxel gets the gray value *GV* obtained by interpolation the gray value gv_1 from the corresponding pixel. (Fig. 5, left)

2. Project every voxel into the second image space. Multiply the existing voxel gray value *GV* with the gray value gv_2 of the corresponding pixel. (Fig. 5, right)
3. Proceed with all other camera views *j*.

Finally, the voxel space will contain multiplicatively accumulated image intensity information of the instantaneous particle constellation. It is obvious, that only voxels at valid particle positions will show high values. Repeating the MART for each epoch results in a time-resolved 3-D voxel space representation of the object space. Disadvantages of a pixel-wise reconstruction and the final realization by the MART can be seen in the computational effort.

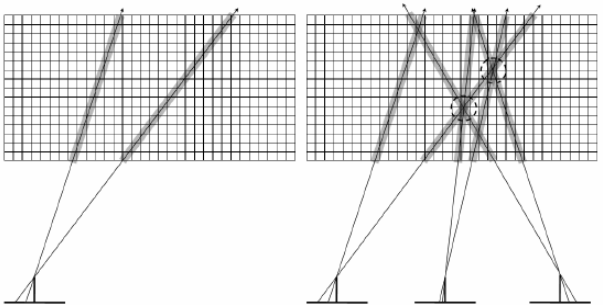

Figure 5: Principle of a tomographic reconstruction (Putze & Maas, 2008)

3.2 Improvements

Improvements can be seen in the radiometric as well as geometric reconstruction process and will be presented and discussed in the following sub-sections.

Algebraic Reconstruction Technique

To fill-up the voxel space with gray value information, Herman and Lent's MART can be replaced by a MinART (minstore algebraic reconstruction technique; Maas et al., 2009) applying a minimum operator rather than a multiplication to the gray values of all camera pixels in each voxel. A 3-D particle constellation can then easily be obtained by a thresholding in voxel space.

Volumetric Reconstruction in Gas

For a volumetric reconstruction in gas, the process bases on a multiple projective transformation of each camera view into each depth layer of a voxel representation of the object space. Compared to pixel-wise line-of-sight based implementations, this approach saves plenty of computation time. After the initialization of the voxel space with an adequate resolution, the calculation of the corresponding image coordinates of each voxel of each depth layer *i* for each view *j* is performed by either using homogeneous coordinates as suggested by Putze & Maas (2008) or even more straightforward by utilizing the projective transformation directly:

$$x' = \frac{a_0 + a_1 X_i + a_2 Y_i}{1 + c_1 X_i + c_2 Y_i} \qquad y' = \frac{b_0 + b_1 X_i + b_2 Y_i}{1 + c_1 X_i + c_2 Y_i} \tag{3}$$

In homogeneous coordinates, it is sufficient to go through the transformation for the corner voxels of a depth layer *i* only. All other image coordinates can be obtained by a bilinear interpolation. See (Putze & Maas, 2008) for a detailed mathematic description.

In the second case, the projective transformation model can be solved directly by taking the four corner voxel of each depth layer *i*. All other image coordinates can be obtained by inserting the corresponding set of parameters into Eq. 3.

A layer-wise reconstruction can be performed with orthographic projections, too. In comparison to the use of a projective transformation, the determination of correspondences between voxel and pixel for each camera view is even more straightforward. Again, only the corner voxel of a depth layer have to be transformed in a discrete way by using the according model equation 1. Due to orthographic projections, all other image coordinates can be obtained by a bilinear interpolation.

Volumetric Reconstruction in Liquid

For a volumetric reconstruction in liquid, the layer-wise rectification approaches are not feasible anymore. To avoid a throwback to a voxel-wise reconstruction from object to image space, the image rays originating in each pixel of each camera are intersected with each layer of the voxel space, taking into account the fact that each ray is twice broken at the air-glass and glass-water interfaces (Sec. 2). Though this solution is performed pixel-wise, it is quite fast. A huge improvement of the computation time can be achieved by thresholding the images before the voxel space transformation, performing the ray tracing only for pixels above the threshold. Obviously, the use of MinART is not feasible here because not every pixel will be projected into the voxel space. As an alternative, the MART can be used.

Further, a volume-wise transformation of each image content into the voxel space can be performed by the determination of the parameters of a polynomial with three variates in *X*, *Y* and *Z* (Eq. 4). Consequently, the use of the improved MinART is feasible again to map the image content into the actual depth layer.

$$x' = \sum_{\alpha\beta\gamma} a_{\alpha\beta\gamma} \cdot X^{\alpha} \cdot Y^{\beta} \cdot Z^{\alpha}, \qquad \alpha, \beta, \gamma \in \mathrm{N} \tag{4}$$

To solve the transformation model of Eq. 4, the image coordinates of a sufficient amount of control points are calculated directly using the collinearity equations 2 plus multimedia correction. The distribution of those control points can be seen in analogy to the distribution of ground control points of a set of aerial photographs for a block adjustment; namely a dense pattern along the edges of the voxel space and some single points in the center of each depth layer. The corresponding image coordinates of all other voxels can then be efficiently calculated by solving Eq. 4 using the set of parameters determined prior.

3.3 Reconstruction Results

The following Fig. 6 shows the reconstruction results at one epoch of a vortex ring in a water tank, illuminated by one of the 10 thickened laser light sheets (Sec. 2). The volumetric representation is 278×1112×944 voxel. Each voxel corresponds to $(90\ \mu m)^3$.

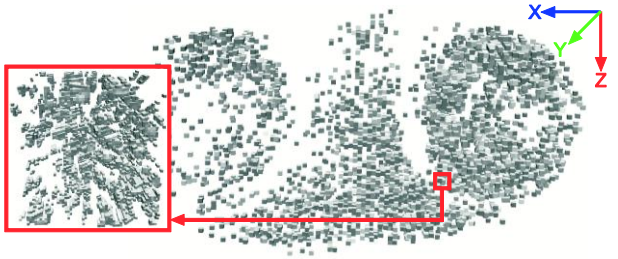

Figure 6. Voxel space of the volumetric reconstruction of a vortex ring at one epoch.

All voxels with gray values less than 15 were eliminated for a better visual representation. Further, the right of Fig. 6 is shows a reduced resolution of 10:1. The section in the left is at full resolution 1:1.

The numeric results of the different geometric reconstruction methods do not differ, which means that the accuracy of the image ray path reconstruction only depends on the accuracy of the calibration routine.

4. VOXEL SPACE TRACKING

4.1 3-D Least Squares Tracking

Eulerian 3-D velocity field information can be obtained by volume-based tracking techniques applied to time-resolved voxel space representations. Here, 3-D least squares tracking (3-D LST) forms a rather interesting alternative to conventional 3-D cross correlation. 3-D LST is a volumetric tracking technique, which is adaptive to cuboid deformation and rotation. It minimizes the sum of the squares of voxel value differences by determining the coefficients of a 3-D affine transformation between cuboids at consecutive time steps. In addition to the three displacement vector components, the 12 parameters of the 3-D affine transformation in 3-D LST contain scale, rotation and shear information. This allows for a higher precision and reliability in case of velocity gradients in the interrogation volume. Moreover, these parameters enable the determination of a shear tensor for each interrogation cube. When applied to liquid flow data, an incompressibility constraint is introduced to force the volume of a cuboid to remain constant during the iterative transformation. The result of 3-D LST applied to sequences of tomographically reconstructed voxel structures is a dense 3-D velocity vector field with additional shear tensor information. A more detailed description of the functional model of the 3-D LST can be found in (Maas et al., 1994).

4.2 Tracking Results

A regular grid of 25^3 voxel cuboids was defined into the volumetric reconstruction gained form Sec. 3 to apply the 3-D LST. For each cuboid, the 12 parameters of the 3-D affine transformation were determined. Parameters, which turned out insignificant in the significance test, were excluded from the transformation. A volume constraint was applied to consider the incompressibility of the liquid. Outliers in the results were removed in an outlier detection procedure based on the following criteria:

- Affine transformation parameter standard deviation: The results of cuboids with standard deviations exceeding a preset threshold were deleted.
- Convergence behavior: Cuboids with a diverging or oscillating solution were rejected.
- Vector length: Translation vectors exceeding a preset threshold were eliminated.
- Neighborhood correlation: The differences of the translation vector components between neighboring cuboids were analyzed. Vectors with deviations from their neighborhood exceeding a preset limit were eliminated.

The 3-D LST steering parameters were set on the basis of a-priori knowledge on the flow and empirically on the basis of a series of program runs. The parameters controlling the outlier elimination process were set automatically following 3-sigma rules. Optionally, gaps in the vector field can be closed by neighborhood based interpolation.

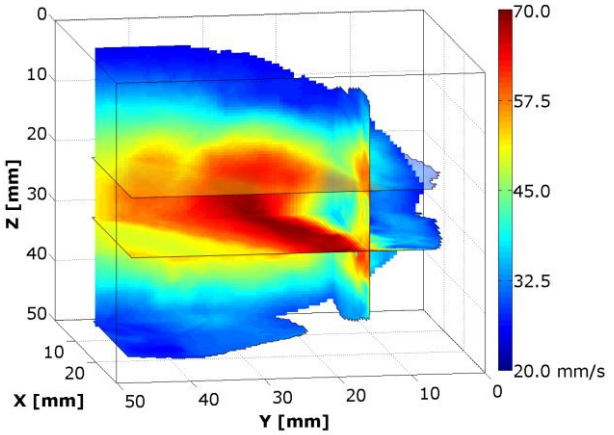

Figure 8. Cross sections of color-coded velocity in voxel space.

Figure 8 shows a color-coded visualization of selected layers in the 3-D LST results. Figure 9 shows the translation vector lengths of one half of the vortex ring in a frontal view. As one can see, some velocity vectors in the center of the vortex were eliminated as potential outliers. This has to be attributed to the finite cuboid size and the fact that the 3-D affine transformation parameters can only recover linear cuboid deformations. The results might be improved by some parameter fine tuning or by a higher seeding density allowing for smaller cuboids.

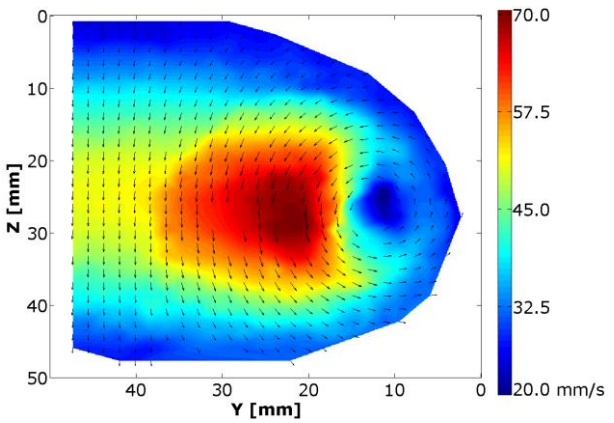

Figure 9. Color-coded vector lengths of one half of the vortex ring (frontal view, X=const.=13.14 mm).

In the experiment described here, the standard deviation of unit weight produced by the least squared adjustment process, averaged over all accepted cuboids, was 2.5 gray values. Tab. 1

shows the average standard deviations of the 12 affine transformation parameters. As one can see, the internal precision of the cuboid translation parameters is in the order of 1/100 of a voxel. However, one has to consider that these internal precision figures are only realistic if the assumed functional and stochastic model is correct (3-D affine transformation and least squares adjustment assuming Gaussian error distribution). Further verification tests have to be performed to get a better estimate of the real accuracy potential of the method.

	a_0	b_0	c_0
σ_i = [vx]	0.0132	0.0105	0.009
Sig = [%]	100	100	100

	a_1	b_2	c_3
σ_i = [vx]	2.4e-3	1.8e-3	1.6e-3
Sig = [%]	1.95	2.68	3.75

	a_2	a_3	b_1	b_3	c_1	c_2
σ_i = [vx]	2.4e-3	2.3e-3	1.7e-3	1.8e-3	1.6e-3	1.6e-3
Sig. = [%]	4.42	10.47	6.40	10.77	6.07	12.61

Table 1 Average standard deviations of transformation parameters and percentage of significant parameters in accepted trajectories.

Furthermore, Tab. 1 gives an overview on the percentage of significant 3-D affine transformation parameters over all accepted cuboids. As the cuboid translation parameters (a_0,b_0,c_0) were not excluded as a rule in the significance tests, they all have 100% here. The scale parameters (a_1,b_2,c_3), constrained by the incompressibility condition, were only significant in relatively few cuboids, while the rotation and shear parameters (a_2,a_3,b_1,b_3,c_1,c_2) were significant especially in the center of the vortex (Fig. 10). In total, about 20% of the cuboids showed at least one significant non-translation parameter, proving the adequateness of the 3-D LST approach. Further, the gained 3-D LST non-translation parameters can be used to estimate the 3-D deformation tensor as well as the 3-D rotational tensor directly (Kitzhofer et al., 2010).

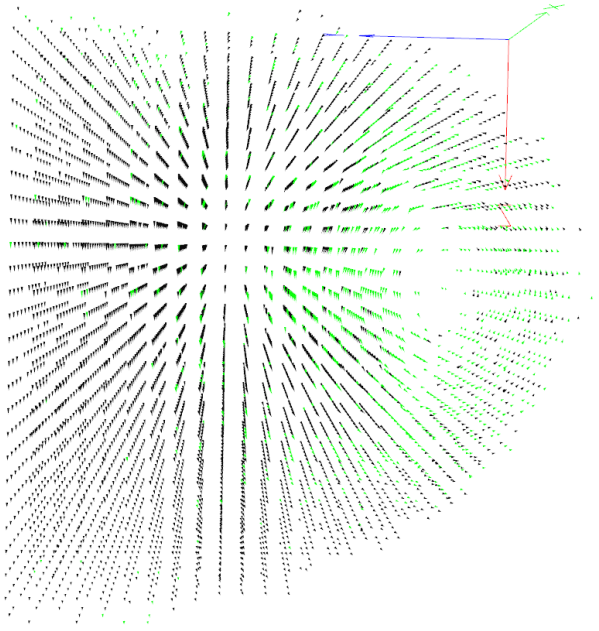

Figure 10. Velocity vector display with vectors belonging to cuboids with at least one significant non-translation 3-D affine transformation parameter coded in green.

5. SUMARY AND OUTLOOK

The suggested approaches for volumetric reconstructions under different experimental setups and 3-D least squares tracking turned out to be efficient and accurate volumetric PIV techniques.

The sequential projective transformation for volumetric reconstructions in gas, resp. in liquids if telecentric lenses are used, has the advantage of being fast and graphics card implementation friendly. For the more common case of a tomographic voxel space reconstruction in liquid using images captured with central perspective lenses, a fast pixel-wise technique and a polynomial approach were proposed. 3-D LST as a cuboid tracking technique has the great advantage of inherently determining 12 affine transformation parameters of each cuboid. These 12 parameters allow to adapt to linear deformations of cuboids, thus improving the precision and reliability of cuboid translation parameters. Moreover, they form a basis for the determination of a shear tensor for each tracked cuboid. The fact that about 20% of tracked cuboids in a vortex ring experiment showed at least one significant non-translation parameter proves the relevance of determining not only transformation parameters in cuboid tracking.

Future work will concentrate on a reliable implementation of the polynomial approach to reconstruct the whole voxel space using one set of higher order polynomial parameters only. Beyond, the linear transformation model in 3-D LST can be extended by introducing higher order polynomials. The resolution of the velocity field may also be improved by identifying individual particles in voxel space and tracking those particles, using the results of the volume-based tracking as good approximation.

ACKNOWLEDGMENTS

The authors would like to thank their cooperation partners Prof. Dr.-Ing. habil Christoph Brücker and Dipl.-Ing. Jens Kitzhofer (Institute of Mechanics and Fluid Dynamics, TU Freiberg, Germany) and Dr.-Ing. Oliver Pust and Thomas I. Nonn (Dantec Dynamics A/S, Skovlunde, Denmark) for providing the vortex ring data set as well as for helpful, supportive and enjoyable suggestions and discussions.

REFERENCES

Elsinga, G. E., Scarano, F., Wieneke, B. & van Oudheusden, B. W., 2005. Tomographic particle image velocimetry. In *6th International Symposium on Particle Image Velocimetry (PIV05)*.

Herman, G. T. & Lent, A., 1976. Iterative reconstruction algorithms. *Computers in Biology and Medicine*, 6:273-294.

Kitzhofer J., Brücker Ch. & Pust O., 2009. Tomo PTV using 3D Scanning Illumination and Telecentric Imaging. *Proceedings of the 8th International Symposium on Particle Image Velocimetry*, 25-28 August, Melbourne, Victoria, Australia.

Kitzhofer, J., Westfeld, P., Pust, O., Maas, H.-G. & Brücker, Ch., 2010. Direct Estimation of 3D Deformation and Rotation Rate Tensor from Gray Value Weighted Voxel Space via Least

Squares Matching. Accepted for publication in the *Proceedings of the 15th International Symposium on Applications of Laser Techniques to Fluid Mechanics*, 5 – 8 July 2010, Lisbon.

Maas, H.-G., Stefanidis, A. & Grün, A., 1994. From pixels to voxels - tracking volume elements in sequences of 3-d digital images. In *International Archives of Photogrammetry and Remote Sensing*, Volume 30, 3/2.

Maas, H.-G., Westfeld, P., Putze, T., Bøtkjær, N., Kitzhofer, J., Brücker, C., 2009. Photogrammetric techniques in multi-camera tomographic PIV. In: Soria, J., Atkinson, C. (eds.), *Proceedings of the 8th International Symposium on Particle Image Velocimetry*, 25-28 August, Melbourne, Victoria, Australia, pp. 599-602.

Mulsow, C., 2010. A Flexible Multi-media Bundle Approach. Accepted for publication in the *Proceedings of the Commission V, WG V/1 Symposium 2010*, 21 – 24 June 2010, Newcastle.

Putze, T. & Maas, H.-G, 2008. 3D determination of very dense particle velocity fields by tomographic reconstruction from four camera views and voxel space tracking. In: Jiang J. Chen J. and H.-G. Maas, editors, *International Archives of Photogrammetry, Remote Sensing and Spatial Information Sciences*, Volume XXXVII, Part B5, pages 33-38. ISPRS.